Inorganic Chemistry

Article

pubs.acs.org/IC

Perovskite-Structure $TlMnO_3$: A New Manganite with New Properties

Wei Yi,[†] Yu Kumagai,[‡] Nicola A. Spaldin,[‡] Yoshitaka Matsushita,[§] Akira Sato,[§] Igor A. Presniakov,[⊥] Alexey V. Sobolev,[⊥] Yana S. Glazkova,[⊥] and Alexei A. Belik*[,†]

[†]International Center for Materials Nanoarchitectonics (WPI-MANA), National Institute for Materials Science (NIMS), 1-1 Namiki, Tsukuba, Ibaraki 305-0044, Japan

[‡]Materials Theory, ETH Zürich, Wolfgang-Pauli-Strasse 27, Zürich 8093, Switzerland

[§]Materials Analysis Station, National Institute for Materials Science, 1-2-1 Sengen, Tsukuba, Ibaraki 305-0047, Japan

[⊥]Department of Chemistry, Lomonosov Moscow State University, Leninskie Gory, 119992 Moscow, Russia

Supporting Information

ABSTRACT: We synthesize a new member of the $AMnO_3$ perovskite manganite family (where A is a trivalent cation)—thallium manganite, $TlMnO_3$—under high-pressure (6 GPa) and high-temperature (1500 K) conditions and show that the structural and magnetic properties are distinct from those of all other $AMnO_3$ manganites. The crystal structure of $TlMnO_3$ is solved and refined using single-crystal X-ray diffraction data. We obtain a triclinically distorted structure with space group $P\bar{1}$ (No. 2), Z = 4, and lattice parameters a = 5.4248(2) Å, b = 7.9403(2) Å, c = 5.28650(10) Å, α = 87.8200(10)°, β = 86.9440(10)°, and γ = 89.3130(10)° at 293 K. There are four crystallographic Mn sites in $TlMnO_3$ forming two groups based on the degree of their Jahn−Teller distortions. Physical properties of insulating $TlMnO_3$ are investigated with Mössbauer spectroscopy and resistivity, specific heat, and magnetization measurements. The orbital ordering, which persists to the decomposition temperature of 820 K, suggests A-type antiferromagnetic ordering with the ferromagnetic planes along the [−101] direction, consistent with the measured collinear antiferromagnetism below the Néel temperature of 92 K. Hybrid density functional calculations are consistent with the experimentally identified structure, insulating ground state, and suggested magnetism, and show that the low symmetry originates from the strongly Jahn−Teller distorted Mn^{3+} ions combined with the strong covalency of the Tl^{3+}−O bonds.

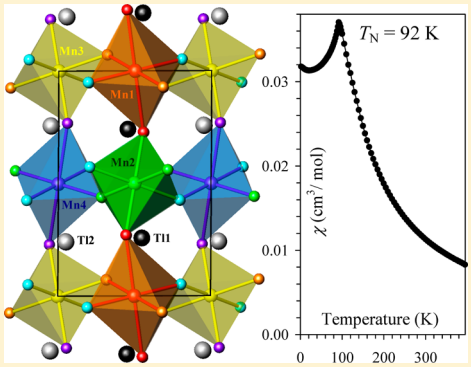

1. INTRODUCTION

Perovskite-structure rare earth manganites, of which $LaMnO_3$ is the prototype, have been a playground for solid-state and materials chemists and physicists for decades.[1−5] Doped $LaMnO_3$-based materials exhibit colossal magnetoresistance,[3,6] a range of charge and orbital orderings,[4] and diverse and coupled ferromagnetic (FM), antiferromagnetic (AFM), insulating, and metallic properties.[1−5] Indeed, even the $LaMnO_3$ end-member can exhibit many of these attractive properties as a result of variations in the oxygen content during the synthesis.[7−9] The undoped manganites $R^{3+}Mn^{3+}O_3$ (with R = rare-earth elements and Y) have been investigated in the context of their multiferroic properties in both perovskite and hexagonal modifications.[10−15] $RMnO_3$ perovskites show rich magnetic phase diagrams,[14] and incommensurate magnetic phases produce ferroelectric polarization for R = Dy and Tb.[10] In addition, the collinear E-type AFM structure adopted by perovskite manganites of the smaller rare earths can also give rise to ferroelectric polarization.[15]

All $RMnO_3$ perovskites (with R = rare-earth elements and Y) crystallize in the $GdFeO_3$-type structure with space group $Pnma$ and the $a^+b^-b^-$ Glazer tilt system.[16,17] All have the same orbital ordering, but the magnitude of octahedral tilt affects the transition metal−oxygen angles, and in turn the magnetic ordering in the ground state: A-type AFM ordering with spin canting is observed for small tilts (R = La−Gd), spin spirals are realized for intermediate tilts (R = Tb and Dy), and E-type AFM ordering without spin canting is observed for larger tilts (R = Ho−Lu).[14,15] The family of trivalent perovskite manganites also includes $BiMnO_3$, which adopts the space group $C2/c$ and has an orbital ordering pattern distinct from that of the rare earth and Y perovskite manganites. ($AMnO_3$ will be used for the extended family of trivalent perovskite manganites beyond rare-earth elements and Y.) Bulk $BiMnO_3$ can only be prepared using high-pressure (HP) high-temperature (HT) techniques, and so its structural and ferroelectric properties were for a long time controversial.[18−20] Intriguingly, $BiMnO_3$ is the only stoichiometric trivalent perovskite manganite with ferromagnetic properties ($T_C \approx$ 100 K), and indeed one of the few known ferromagnetic insulators.[19]

There is therefore considerable motivation to extend the perovskite $AMnO_3$ family in the search for new magneto-structural coupling behaviors. Unfortunately, however, few

Received: June 12, 2014
Published: August 27, 2014

   dx.doi.org/10.1021/ic501380m | Inorg. Chem. 2014, 53, 9800−9808

possibilities remain. Recent attempts include the stabilization of $(In_{1-y}Mn_y)MnO_3$ $(1/9 \le y \le 1/3)$,[21] $ScMnO_3$,[22] and even Mn_2O_3[23] perovskites using the HP-HT technique.[24] In $(In_{1-y}Mn_y)MnO_3$,[21] however, it was found that the *A*-site Mn ions are divalent, resulting in *B*-site doping and ordering, and so it belongs to the doped manganites rather than the trivalent $AMnO_3$ family. Interestingly, $ScMnO_3$ perovskite is isostructural with $(In_{1-y}Mn_y)MnO_3$,[22] showing two crystallographic Mn sites with quite different Jahn–Teller distortions, and so is likely also a doped manganite. We point out that $ScMnO_3$ and $InMnO_3$ crystallize in the same nonperovskite hexagonal structure[25,26] adopted by the $RMnO_3$ perovskites with smaller *A*-site cations (*R* = Y and Ho–Lu) if they are not synthesized under HP-HT conditions.[25] Finally, Mn_2O_3 actually forms as $[MnMn_3]Mn_4O_{12}$, with larger Mn^{2+} ions occupying the perovskite *A* site giving an *A*-site ordered structure,[23] and so also cannot be considered a member of the $AMnO_3$ family. A very limited number of elements still remain for the expansion of the $AMnO_3$ family, with Al^{3+}, Ga^{3+}, Sb^{3+}, and Tl^{3+} being possible trivalent candidates.[24] Al^{3+} and Ga^{3+} ions are too small for stabilization of perovskite structures and synthesis of $AlMnO_3$ and $GaMnO_3$ perovskites would likely require prohibitively high pressures. While Sb^{3+} ions are larger, they would also need HP-HT growth, but under such conditions they might be unstable relative to disproportionation into Sb^0 and Sb^{5+}, especially in contacts with capsule materials. We explore the remaining possibility—$TlMnO_3$—here.

$TlMO_3$ perovskites (where *M* is a transition metal) have been synthesized under HP-HT conditions and studied for *M* = Cr, Fe, and Ni.[27−30] $TlCrO_3$, $TlFeO_3$, and $TlNiO_3$ perovskites were found to crystallize in $GdFeO_3$-type structures similar to the corresponding $RCrO_3$, $RFeO_3$, and $RNiO_3$ families (*R* = Y and rare earths),[27−30] and $TlNiO_3$ has a monoclinic distortion from charge disproportionation of Ni^{3+} ions.[30] Because of the strong covalency of the Tl–O bonds, there are some peculiarities in the crystallographic and magnetic properties of $TlFeO_3$ and $TlNiO_3$.[28−30] In particular, the Néel temperatures of $TlFeO_3$ and $TlNiO_3$ are much smaller than those of the corresponding $RFeO_3$ and $RNiO_3$ families (*R* = Y and rare earths), and the unit cell volumes of $TlFeO_3$ and $TlNiO_3$ are close to those of $DyFeO_3$ and $DyNiO_3$, respectively, while the Shannon ionic radius of Tl^{3+} (r_{VIII} = 0.98 Å) is smaller than that of Dy^{3+} (r_{VIII} = 1.027 Å) and is in fact closer to that of Lu^{3+} (r_{VIII} = 0.977 Å).[31] For $TlCrO_3$, only the lattice parameters but no properties have been reported.[27] $TlMnO_3$ was mentioned in ref 32; however, no information on $TlMnO_3$ (such as purity, lattice parameters, and properties) was reported.

In this work, we describe the HP-HT synthesis, crystal structure, and properties of a new member of the $AMnO_3$ perovskite manganite family, $TlMnO_3$. We find that $TlMnO_3$ forms in a highly distorted variant of the perovskite structure with $P\bar{1}$ symmetry, and is antiferromagnetic with a Néel temperature of 92 K. The local structure is studied by Mössbauer spectroscopy in the iron-doped $TlMn_{0.99}{}^{57}Fe_{0.01}O_3$ and $TlMn_{0.95}{}^{57}Fe_{0.05}O_3$. To confirm and explain the experimental findings we perform state-of-the-art density functional calculations using hybrid functionals, and show that the distorted structure arises from a combination of the Jahn–Teller distortions around the Mn^{3+} ions and the strongly covalent Tl^{3+}-O bonds, which cause the Tl^{3+} ions to adopt a locally distorted environment. Our calculations indicate an A-type antiferromagnetic ordering with [−101] ferromagnetically aligned planes, consistent with the observed orbital ordering.

2. EXPERIMENTAL AND COMPUTATIONAL DETAILS

Caution! *Thallium and its compounds are highly toxic.* $TlMnO_3$ was prepared from a stoichiometric mixture of Mn_2O_3 (prepared from commercial MnO_2 (99.99%) by heating in air at 923 K for 24 h) and Tl_2O_3 (99.99%) taking care because of the high toxicity of thallium and its compounds. The mixture was placed in Au capsules and treated at 6 GPa in a belt-type high-pressure apparatus at 1500 K for 2 h (heating rate to the desired temperature was 10 min). After the heat treatment, the samples were quenched to room temperature (RT), and the pressure was slowly released. The $TlMnO_3$ samples were black fragile pellets, stable in air, with single crystals found in some samples. $TlMn_{0.99}{}^{57}Fe_{0.01}O_3$ and $TlMn_{0.95}{}^{57}Fe_{0.05}O_3$ were prepared using the same method from stoichiometric mixtures of Mn_2O_3, Tl_2O_3, and $^{57}Fe_2O_3$. The lattice parameters were a = 5.4206(2) Å, b = 7.9296(2) Å, c = 5.2845(2) Å, α = 87.883(4)°, β = 87.046(4)°, and γ = 89.342(4)° for $TlMn_{0.99}{}^{57}Fe_{0.01}O_3$ and a = 5.4243(2) Å, b = 7.9275(2) Å, c = 5.2894(2) Å, α = 87.920(4)°, β = 87.098(4)°, and γ = 89.367(4)° for $TlMn_{0.95}{}^{57}Fe_{0.05}O_3$.

X-ray powder diffraction (XRPD) data of $TlMnO_3$ collected at RT on a RIGAKU Ultima III diffractometer using Cu Kα radiation (2θ range of 10–100°, a step width of 0.02°, and a counting time of 12 s/step) showed that the samples contained small amounts of $Tl_2Mn_2O_7$ and Tl_2O_3 impurities (see Supporting Information).

Synchrotron XRPD data were measured at 293 K on a large Debye–Scherrer camera at the BL15XU beamline of SPring-8.[33] The intensity data were collected between 2° and 60° at 0.003° intervals in 2θ; the incident beam was monochromatized at λ = 0.652 97 Å. The sample was packed into a Lindenmann glass capillary (inner diameter: 0.1 mm), which was rotated during the measurement. The absorption coefficient was also measured, and Rietveld analysis was applied using the RIETAN-2000 program.[34]

X-ray single-crystal intensity data were collected at 293 K using a Bruker SMART APEX single-crystal diffractometer equipped with a CCD area detector and a graphite monochromator utilizing Mo Kα radiation (λ = 0.710 73 Å). Cell parameters were retrieved using SMART software[35] and refined using SAINT software[36] on all observed reflections. Data reduction was performed with SAINT software, which corrects for Lorentz polarization and decay. Absorption corrections were applied using SADABS.[37] Measurement, crystal, and refinement parameters are listed in Table 1. The crystal structure was solved by the direct method with SHELXS-97[38] and

Table 1. Crystal Data and Structural Refinement Parameters for $TlMnO_3$

ideal formula	$TlMnO_3$
empirical formula	$Tl_{0.978}MnO_3$
F_w	302.82
radiation (Å)	0.710 73 (Mo Kα)
instrument	Bruker SMART APEX
temperature (K)	293(2)
space group	$P\bar{1}$ (No. 2)
a (Å)	5.4248(2)
b (Å)	7.9403(2)
c (Å)	5.286 50(10)
α (deg)	87.8200(10)
β (deg)	86.9440(10)
γ (deg)	89.3130(10)
V (Å^3)	227.214(11)
Z	4
ρ_{cal} (g/cm^3)	8.984
F_{000}	520
μ(Mo Kα) (mm^{-1})	76.083
independent reflections [$I > 2\sigma(I)$]	2340
R_{int}; R_1	0.0463; 0.0359
wR_2; GOF	0.0895; 1.034

dx.doi.org/10.1021/ic501380m | Inorg. Chem. 2014, 53, 9800–9808

Table 2. Structural Parameters of $TlMnO_3$ at Room Temperature

site	WP[a]	g[a]	x	y	z	100 × U_{equiv} (Å^2)
Tl1	2*i*	0.978(6)	0.54745(4)	0.257 94(3)	0.509 94(4)	0.498(7)
Tl2	2*i*	0.978(6)	0.049 35(4)	0.242 33(3)	0.975 13(4)	0.438(7)
Mn1	1*d*	1	0.5	0	0	0.37(2)
Mn2	1*e*	1	0.5	0.5	0	0.30(2)
Mn3	1*b*	1	0	0	0.5	0.34(2)
Mn4	1*g*	1	0	0.5	0.5	0.40(2)
O1	2*i*	1	0.9423(8)	0.2309(5)	0.3799(8)	0.60(7)
O2	2*i*	1	0.4450(7)	0.2708(5)	0.1147(8)	0.52(6)
O3	2*i*	1	0.2056(8)	0.5732(6)	0.2055(9)	0.85(7)
O4	2*i*	1	0.8053(8)	0.0511(6)	0.8070(8)	0.68(7)
O5	2*i*	1	0.2824(8)	0.4406(6)	0.6847(9)	0.87(7)
O6	2*i*	1	0.6839(8)	0.9275(6)	0.2855(8)	0.63(7)

[a]WP is Wyckoff position; *g* is the occupation factor.

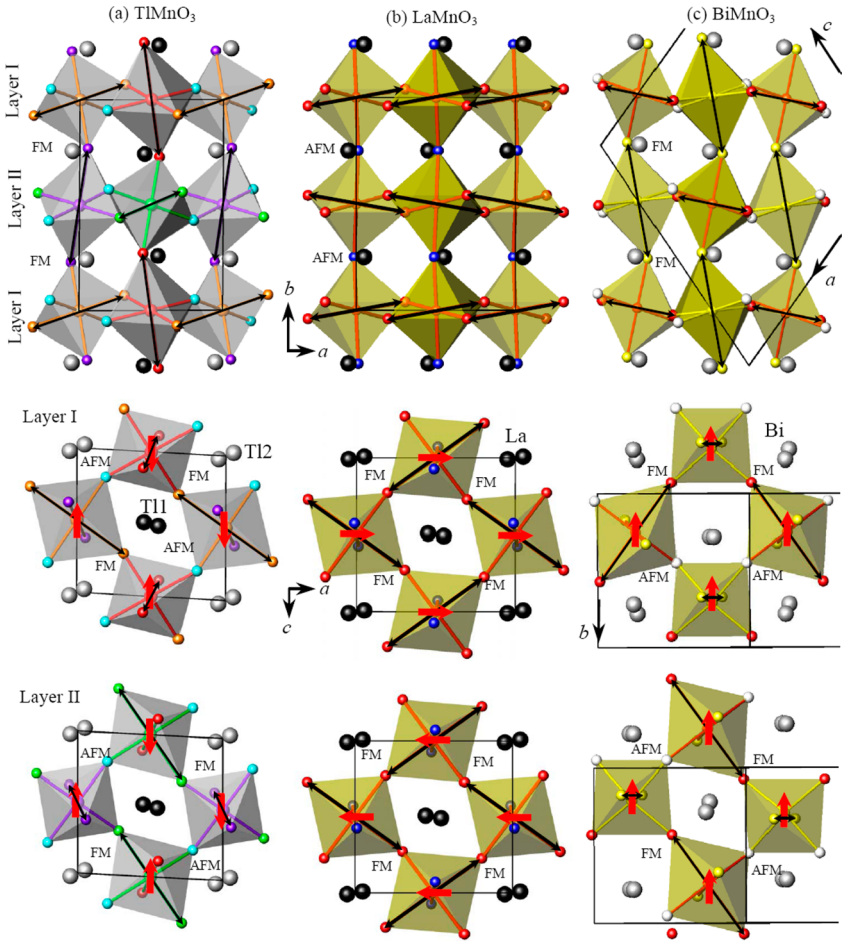

Figure 1. Crystal structures of (a) $TlMnO_3$, (b) $LaMnO_3$,[50] and (c) $BiMnO_3$[18] along different directions. The longest Mn−O bonds are shown by double-headed black arrows. Bold red arrows give schematic magnetic structures (from the literature for $LaMnO_3$[9] and $BiMnO_3$,[59,60] and proposed here for $TlMnO_3$). FM and AFM give the type of magnetic interactions based on the orbital arrangement.

subsequently refined against all data in the 2θ ranges by full-matrix least-squares on F^2 using SHELXL-97,[38] working on WinGX suite.[39]

Magnetic susceptibilities ($\chi = \mathbf{M}/\mathbf{H}$) were measured using a SQUID magnetometer (Quantum Design, MPMS) between 2 and 400 K in different applied magnetic fields under both zero-field-cooled (ZFC) and field-cooled (FC, on cooling) conditions. Isothermal magnetization measurements were performed between −70 and 70 kOe at 5 K. Specific heat, C_p, was recorded between 2 and 300 K on cooling at 0 and 70 kOe by a pulse relaxation method using a commercial calorimeter (Quantum Design PPMS). dc electrical resistivity of single crystals was measured from 350 K down to about 200 K by the conventional four-probe method using a Quantum Design PPMS; resistivity became too high to be measured with our system below 200 K. The resistivity at RT was about 10^3 Ω cm, and the activation energy was about 0.28 eV (see the Supporting Information). Differential scanning calorimetry (DSC) curves of $TlMnO_3$ powder were recorded on a Mettler Toledo DSC1 STAR^e system at a heating/cooling rate of 10 K/min between 290 and 973 K in open Pt capsules. Dielectric properties were measured using an Agilent E4980A LCR meter between 5 and 300 K in the frequency range of 1 kHz and 1 MHz; no dielectric anomalies were observed.

dx.doi.org/10.1021/ic501380m | Inorg. Chem. 2014, 53, 9800−9808

Table 3. Selected Bond Lengths (l (Å) < 3.2 Å), Bond Valence Sums (BVS), Bond Angles (deg), and Distortion Parameters of MnO_6 Octahedra (Δ(Mn)) in $TlMnO_3$[a]

Tl1−O6	2.166(4)	Tl2−O1	2.186(4)
Tl1−O2	2.189(4)	Tl2−O3	2.226(4)
Tl1−O5	2.221(4)	Tl2−O4	2.264(5)
Tl1−O1	2.225(4)	Tl2−O2	2.323(4)
Tl1−O3	2.503(5)	Tl2−O6	2.386(5)
Tl1−O4	2.665(4)	Tl2−O5	2.468(5)
Tl1−O5	2.721(5)	Tl2−O4	2.688(4)
Tl1−O6	2.989(5)	Tl2−O3	3.084(5)
BVS($Tl1^{3+}$)	2.99	BVS($Tl2^{3+}$)	2.92
Mn1−O6 (× 2)	1.920(4)	Mn2−O2 (× 2)	1.918(4)
Mn1−O4 (× 2)	1.937(4)	Mn2−O3 (× 2)	1.977(4)
Mn1−O2 (× 2)	2.268(4)	Mn2−O5 (× 2)	2.163(5)
BVS($Mn1^{3+}$)	3.04	BVS($Mn2^{3+}$)	3.09
Δ(Mn1) × 10^4	61.6	Δ(Mn2) × 10^4	26.7
Mn3−O4 (× 2)	1.942(4)	Mn4−O5 (× 2)	1.905(4)
Mn3−O1 (× 2)	1.945(4)	Mn4−O3 (× 2)	1.941(4)
Mn3−O6 (× 2)	2.199(4)	Mn4−O1 (× 2)	2.282(4)
BVS($Mn3^{3+}$)	3.05	BVS($Mn4^{3+}$)	3.07
Δ(Mn3) × 10^4	35.3	Δ(Mn4) × 10^4	69.2
Mn1−O2−Mn2 (× 2)	142.9(2)	Mn2−O3−Mn4 (× 2)	140.3(2)
Mn1−O4−Mn3 (× 2)	143.6(3)	Mn2−O5−Mn4 (× 2)	145.6(2)
Mn1−O6−Mn3 (× 2)	141.2(2)	Mn3−O1−Mn4 (× 2)	139.7(2)
		<Mn−O−Mn>	142.2

[a]BVS = $\Sigma_{i=1}^{N}\nu_i$, where $\nu_i = \exp[(R_0 - l_i)/B]$, N is the coordination number, B = 0.37, $R_0(Tl^{3+})$ = 2.003, $R_0(Mn^{3+})$ = 1.76.[49]

^{57}Fe Mössbauer spectra were recorded at 10 and 300 K using a conventional constant-acceleration spectrometer. The radiation source ^{57}Co(Rh) was kept at RT. All isomer shifts are referred to α-Fe at 300 K. The experimental spectra were processed and analyzed using methods of spectral simulations implemented in the SpectrRelax program.[40]

First-principles calculations were performed using density functional theory within the projector-augmented wave method[41] as implemented in the VASP code.[42] The exchange-correlation interactions among electrons were treated using the Heyd−Scuseria−Ernzerhof (HSE06) hybrid functional,[43] which is well-recognized to show accurate magnetic, electronic, and structural properties in insulating transition metal compounds.[44−48] An energy cutoff of 600 eV was employed, and lattice constants and internal atomic positions were fully relaxed until the forces and stresses were less than 0.005 eV/Å and 0.034 GPa. Tl $5d^{10}$, $6s^2$, and $6p^1$, Mn $3d^5$ and $4s^2$, and O $2s^2$ and $2p^4$ electrons were treated as valence electrons.

3. RESULTS

Our measured structural parameters of $TlMnO_3$ are summarized in Table 2, and a picture of the corresponding crystal structure is shown in Figure 1. One can see from Figure 1a,b that $TlMnO_3$ adopts a tilt pattern, which is common to many $RMnO_3$ compounds, but with an additional symmetry-lowering triclinic distortion. That results in the $a^+b^-c^-$ tilt system. The structural parameters deduced from the synchrotron XRPD data are given in the Supporting Information. A small deficiency at the Tl sites was observed from single-crystal and synchrotron XRPD data, consistent with the presence of small amounts of Tl_2O_3 impurities. In Table 3 we list the primary bond lengths, bond-valence sums (BVS)[49] and distortion parameters of MnO_6 octahedra (Δ_d(Mn)).[50] The BVS values of all the sites are close to the formal ionic values of +3. All MnO_6 octahedra exhibit strong Jahn−Teller distortions, with two of the Δ_d parameters in $TlMnO_3$ (Δ_d(Mn1) = 61.6 × 10^{-4} and Δ_d(Mn4) = 69.2 × 10^{-4}) being much larger than that of $LaMnO_3$ at 300 K (Δ_d(Mn) = 33.1 × 10^{-4}),[50] and comparable with that of $TmMnO_3$ (Δ_d(Mn) = 64.4 × 10^{-4}).[14] The other two Δ_d parameters (Δ_d(Mn2) = 26.7 × 10^{-4} and Δ_d(Mn3) = 35.3 × 10^{-4}) are comparable with that of $LaMnO_3$. No DSC anomalies were observed below 800 K indicating the absence of any structural phase transitions, and so the orbital ordering of the Jahn−Teller distortions must persist to this temperature. Note that the orbital-ordering temperature (T_{OO}) is 750 K in $LaMnO_3$, and it increases to about 900 K in $PrMnO_3$ and above 1000 K in $NdMnO_3$.[50−52] But T_{OO} is just 474 K in $BiMnO_3$.[18] At 820 K, a DSC anomaly was observed in $TlMnO_3$ (see Supporting Information) corresponding to decomposition of the sample (see XRPD data after heating to 873 K in the Supporting Information).

Our measured magnetic susceptibilities of $TlMnO_3$ showed almost no difference between the ZFC and FC curves. At small magnetic field values, a contribution from the FM $Tl_2Mn_2O_7$ impurity with T_C = 158 K (note that $Tl_2Mn_2O_7$ can also be prepared only at HP-HT conditions)[53,54] is visible (see the Supporting Information). However, at larger magnetic fields (e.g., 70 kOe; Figure 2a), the contribution from $Tl_2Mn_2O_7$ is completely suppressed. Both ZFC and FC susceptibilities have sharp peaks typical for antiferromagnets near 92 K. The inverse ZFC magnetic susceptibilities (at 70 kOe) between 250 and 400 K were fit by the Curie−Weiss equation

$$\chi(T) = \mu_{eff}^2 N(3k_B(T - \theta))^{-1} \quad (1)$$

where μ_{eff} is the effective magnetic moment, N is Avogadro's number, k_B is Boltzmann's constant, and θ is the Weiss constant. We obtained values (Figure 2a) of μ_{eff} = 4.897(3)μ_B, close to the ideal localized Mn^{3+} moment of 4.899 μ_B, and θ = +32.1(3) K, indicating that the dominant interaction between Mn^{3+} ions is FM. Note that a positive Curie−Weiss temperature of 46−52 K was also observed in $LaMnO_3$,[51,55] which has an AFM spin structure (Figure 1b) with small spin canting. The specific heat shows typical sharp anomalies near

dx.doi.org/10.1021/ic501380m | Inorg. Chem. 2014, 53, 9800−9808

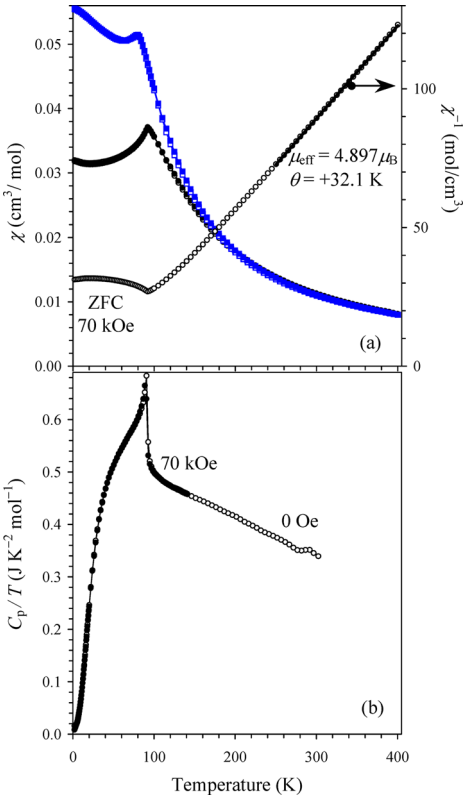

Figure 2. (a) ZFC (white symbols) and FC (filled symbols) direct current magnetic susceptibility ($\chi = M/H$) curves of $TlMnO_3$ (circles) and $TlMn_{0.95}{}^{57}Fe_{0.05}O_3$ (squares) at 70 kOe (the left-hand axis) and the ZFC inverse curve (χ^{-1} vs T) of $TlMnO_3$ (the right-hand axis). The parameters (μ_{eff} and θ) of the Curie–Weiss fit between 250 and 400 K are given. (b) Specific heat data of $TlMnO_3$ at zero magnetic field (○) and 70 kOe (●) plotted as C_p/T vs T.

T_N (Figure 2b) indicating the onset of long-range magnetic ordering. A magnetic field of 70 kOe had almost no effect on the anomalies near T_N indicating the robustness of the AFM state. The M versus H curves of $TlMnO_3$ at 5 K were linear with a small kink near the origin (Figure 3) originating from the soft FM $Tl_2Mn_2O_7$ impurities.[53,54] A linear extrapolation between 20 and 70 kOe gives the saturation magnetization of the impurity as $0.0170(3)\mu_B$/f.u., corresponding to 0.28 mol % $Tl_2Mn_2O_7$ with the full saturation of 6 μ_B/f.u. The M versus H

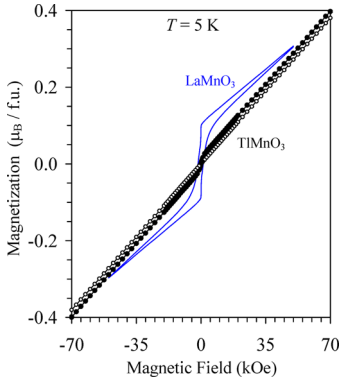

Figure 3. M vs H curves of $TlMnO_3$ (symbols) and $LaMnO_3$ (blue line) at 5 K. Black symbols give the original data for $TlMnO_3$; white symbols give the data corrected for the $Tl_2Mn_2O_7$ ferromagnetic impurity with the saturation magnetization of 0.017 μ_B/f.u.

curves showed that $TlMnO_3$ is a fully compensated antiferromagnet without weak ferromagnetism from spin canting. The T_N drops to 89 K in $TlMn_{0.99}{}^{57}Fe_{0.01}O_3$ (see Supporting Information) and to 78 K in $TlMn_{0.95}{}^{57}Fe_{0.05}O_3$ (Figure 2a). It is interesting that the iron doping increases the magnetic transition temperature in $BiMn_{1-x}Fe_xO_3$ from 100 K for x = 0 to 110 K for x = 0.05.[56]

The ^{57}Fe Mössbauer spectra of $TlMn_{0.99}{}^{57}Fe_{0.01}O_3$ and $TlMn_{0.95}{}^{57}Fe_{0.05}O_3$ at 300 K consist of asymmetric paramagnetic doublets with broadened components (Figure 4).

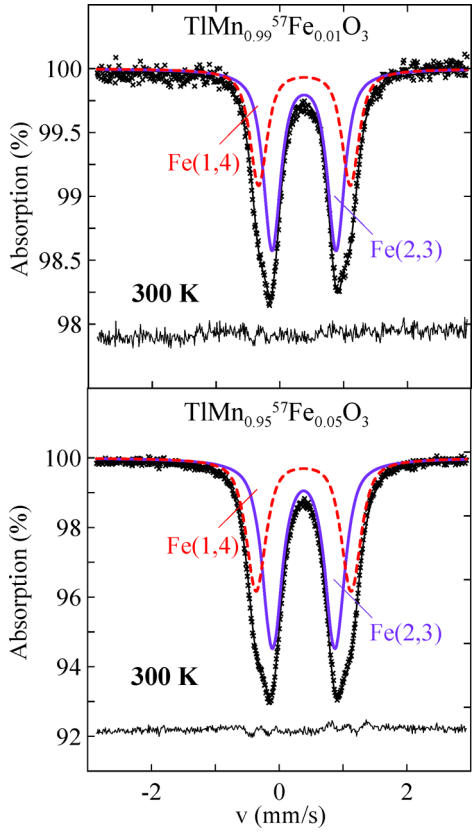

Figure 4. ^{57}Fe Mössbauer spectra at 300 K and fitting results with two doublets for $TlMn_{0.99}{}^{57}Fe_{0.01}O_3$ and $TlMn_{0.95}{}^{57}Fe_{0.05}O_3$.

The distribution function $p(\Delta)$ of the quadrupole splitting (Δ) has been restored to select fitting models. The resulting $p(\Delta)$ has two main peaks (see Supporting Information), indicating that $^{57}Fe^{3+}$ ions occupy two nonequivalent positions, Fe(1,4) and Fe(2,3), with the average Δ values of 1.52 and 1.02 mm/s, respectively. On the basis of the $p(\Delta)$ profile analysis, we described the experimental spectra as a superposition of two quadrupole doublets, Fe(1,4) and Fe(2,3), with very close values of isomer shifts ($\delta_{(1,4)} \approx \delta_{(2,3)}$) and constrained line width ($W_{(1,4)} = W_{(2,3)}$), but with significantly different quadrupole splitting. The resulting hyperfine parameters (δ, Δ, W) and relative intensities (I) are listed in Table 4. All the parameters were the same within standard deviations independent of the iron content (1% or 5%). The isomer shifts of the Fe(1,4) and Fe(2,3) doublets correspond to the high-spin Fe^{3+} ($3d^5$, S = 5/2) ions in octahedral oxygen coordination. Their different quadrupole splitting values could originate from quite different octahedral distortions of $Mn1O_6$/$Mn4O_6$ and $Mn2O_6$/$Mn3O_6$ octahedra in $TlMnO_3$. To confirm this, we calculated a lattice contribution to the electric

dx.doi.org/10.1021/ic501380m | Inorg. Chem. 2014, 53, 9800–9808

Table 4. Hyperfine Parameters of the ^{57}Fe Mössbauer Spectra of $TlMn_{0.99}{}^{57}Fe_{0.01}O_3$ and $TlMn_{0.95}{}^{57}Fe_{0.05}O_3$ at 300 K

sample	sites	δ^a (mm/s)	Δ^a (mm/s)	W^a (mm/s)	I^a (%)
$TlMn_{0.99}{}^{57}Fe_{0.01}O_3$	Fe(1,4)	0.39(2)	1.44(3)	0.32(2)^b	39(3)
	Fe(2,3)	0.39(2)	1.01(2)	0.32	61(3)
$TlMn_{0.95}{}^{57}Fe_{0.05}O_3$	Fe(1,4)	0.38(2)	1.48(3)	0.37(2)^b	42(2)
	Fe(2,3)	0.38(2)	0.98(2)	0.37	58(2)

$^a\delta$ is an isomer shift, Δ is quadrupole splitting, W is line width, and I is a relative intensity. ^bW parameters were constrained to be the same for the Fe(1,4) and Fe(2,3) sites.

field gradient tensor at $^{57}Fe^{3+}$ ions based on the structural data for undoped $TlMnO_3$ (see Supporting Information for calculation details). The calculated $\Delta_{(1,4)}/\Delta_{(2,3)}$ ratio of 1.30 is in good agreement with the experimental one of 1.43 (for $TlMn_{0.99}{}^{57}Fe_{0.01}O_3$). We note that based on the I values, $^{57}Fe^{3+}$ ions preferably occupy the less distorted Mn2 and Mn3 positions. At 10 K, the Mössbauer effect was too weak in $TlMn_{0.99}{}^{57}Fe_{0.01}O_3$; therefore, only $TlMn_{0.95}{}^{57}Fe_{0.05}O_3$ was investigated whose spectrum is given in Figure 5; this result confirmed the appearance of long-range magnetic ordering.

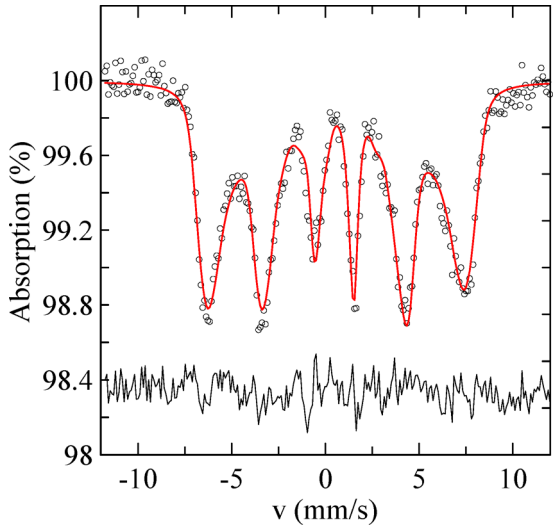

Figure 5. ^{57}Fe Mössbauer spectrum of $TlMn_{0.95}{}^{57}Fe_{0.05}O_3$ at 10 K.

To understand the structure and magnetism we performed density functional calculations as described in the Methods section. We began by analyzing the likely magnetic order starting from the orbital ordering revealed by the experimentally observed elongations of the MnO_6 octahedra (Figure 1). According to the Goodenough–Kanamori rules, the superexchange interaction between Mn^{3+} ($t_{2g}{}^3e_g{}^1$) ions is AFM if both occupied e_g orbitals lie perpendicular to the bond direction, and FM if one of the e_g orbitals lies perpendicular and one along the bond direction. Therefore, by inspection, we expect each Mn ion in $TlMnO_3$ to have four FM neighbors, in the [010] and [101] directions, and two AFM neighbors perpendicular to the FM planes leading to a [−101] A-type AFM ordering. Such a magnetic ordering requires a unit cell that is doubled along two axes relative to the crystallographic unit cell, and therefore by symmetry cannot support weak ferromagnetism.[57] To verify the expected magnetic ordering, we calculated the energy of all eight collinear magnetic orderings compatible with the 20-atom structural unit cell by fully relaxing the structure in each case, that is, FM, three types of AFM (A, C, and G), and four ferrimagnetic (FerriM) orderings as well as the expected [−101] A-type AFM ordering, which we modeled with an 80-atom 2 × 1 × 2 supercell of the 20-atom structural unit. For reciprocal space integration, Γ-centered 4 × 3 × 4 and 2 × 3 × 2 k-point meshes were adopted for the primitive unit cell and 2 × 1 × 2 supercell, respectively. Comparing the total energies, we indeed find that the [−101] AFM ordering is the lowest energy, with the FM arrangement the next lowest (0.24 meV/f.u. higher in energy), and the other magnetic orderings showing much higher energies (Figure 6). Since the FM state is inconsistent with our measurements, we conclude that the most likely magnetic configuration is the [−101] AFM consistent with the orbital ordering analysis. Our calculated lattice constants and internal positions of all ions (see Supporting Information) for the [−101] AFM ordering agree well with the experimental values confirming the validity of our HSE06 hybrid functional calculations. The small energy difference between the [−101] AFM and FM magnetic structures suggests that ferromagnetism might easily be induced in $TlMnO_3$ by different modifications similar to $LaMnO_{3+\delta}$ and $La_{1-x}Sr_xMnO_3$.[1,5,7−9] Note that A-type AFM along the b direction (AFM-I in Figure 6), which is stable in $LaMnO_3$, is much higher in energy, indicating the strong stability of the FM interaction along the b direction. The A-type AFM ordering in $TlMnO_3$ is supported by the absence of weak ferromagetism[57] and by the absence of dielectric anomalies at T_N.

Finally, in Figure 7, we show our calculated density of states (DOS) for $TlMnO_3$ with the ground state [−101] AFM ordering. The valence bands consist mainly of Mn-d (four majority-spin) and O-2p states. The Tl semicore 5d states form a narrow band that is around −11.5 eV below the top of the valence band. They do not directly contribute to covalent bonding with the oxygen anions. Notably, the energies of the formally unoccupied Tl 6s and 6p states are substantially lower than expected: The Tl 6s and 6p states, which would be completely empty in the ionic limit, develop significant occupation through Tl–O 2p covalency and form the bottom of the valence band. Such covalent bonding–which persists in calculations for the high symmetry reference cubic phase–favors a low symmetry environment to optimize Tl–O bonding, and is likely responsible for the low structural symmetry of $TlMnO_3$. Both VBM and CBM are located in the Γ point giving a direct band gap of about 1.3 eV.

4. DISCUSSION—COMPARISON TO OTHER TRIVALENT PEROVSKITE MANGANITES

Finally, we compare the behavior of $TlMnO_3$ to that of the other rare earth trivalent perovskite manganites and $BiMnO_3$. We begin with the structural properties. Since it is difficult to compare the lattice parameters because of the very strong triclinic distortion in $TlMnO_3$, in Figure 8 we compare the unit cell volumes, plotted as a function of ionic radius. We see that the unit cell volume of $TlMnO_3$ (V = 227.2 Å^3) is close to that

dx.doi.org/10.1021/ic501380m | Inorg. Chem. 2014, 53, 9800–9808

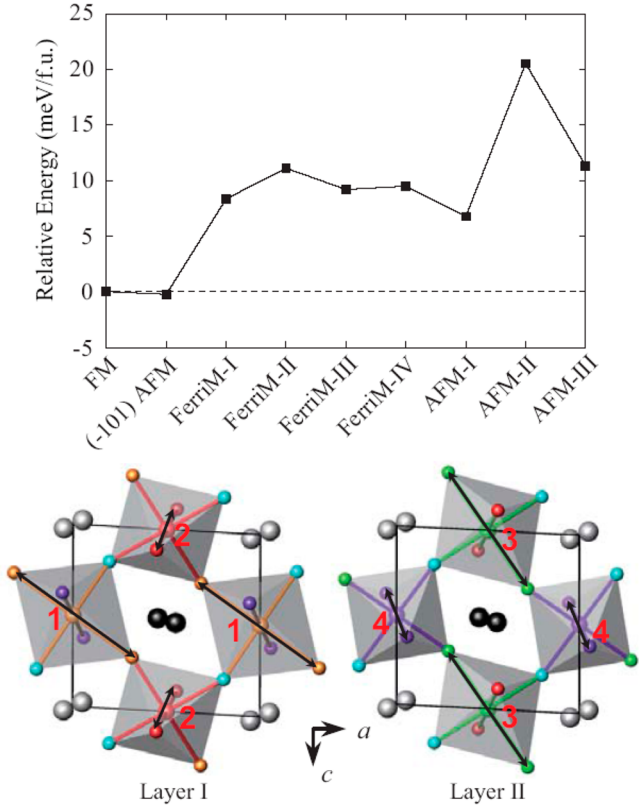

	1	2	3	4
FerriM-I	up	up	up	down
FerriM-II	up	up	down	up
FerriM-III	up	down	up	up
FerriM-IV	down	up	up	up
AFM-I	up	up	down	down
AFM-II	up	down	up	down
AFM-III	up	down	down	up

Figure 6. Calculated relative energy of different magnetic configurations relative to FM ordering in $TlMnO_3$. AFM-I, AFM-II, and AFM-III correspond to A-type AFM along the *b* direction, G-type AFM, and C-type AFM along the (101) direction, respectively.

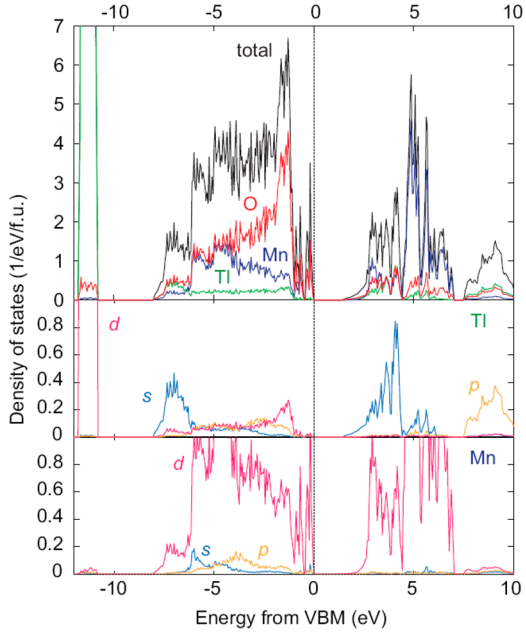

Figure 7. Calculated density of states for $TlMnO_3$ with [−101] AFM ordering. The zero of energy is set to the top of the valence band. The valence band is composed mainly of O 2p and Mn 3d orbitals, with contributions from the formally unoccupied Tl 6s and −6p orbitals at the bottom.

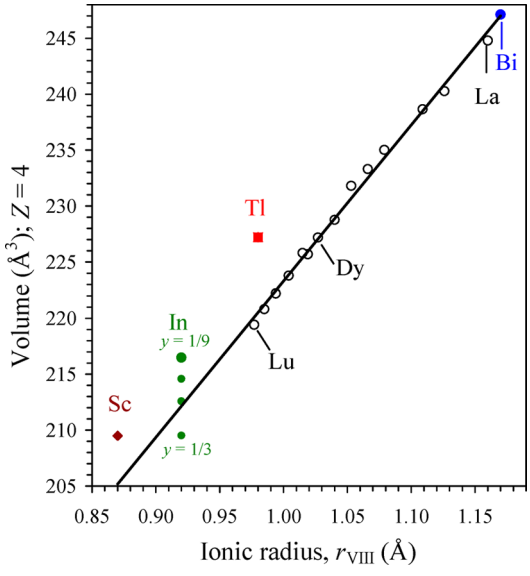

Figure 8. Room-temperature unit cell volume (with $Z = 4$) vs the Shannon ionic radius[31] of $TlMnO_3$ (space group $P\bar{1}$), $BiMnO_3$ (space group $C2/c$),[18] $ScMnO_3$ (space group $P2_1/n$),[22] $(In_{1-y}Mn_y)MnO_3$ ($1/9 \le y \le 1/3$) (space group $P2_1/n$),[21] and $RMnO_3$ (R = La−Lu) (space group *Pnma*)[14] perovskites.[24] The solid line is the least-squares linear fit of the data for $RMnO_3$ (*R* = La−Lu).

of $DyMnO_3$ (V = 227.2 Å^3). As mentioned above, the same tendency was noted previously for $TlCrO_3$ and $DyCrO_3$ (219.1 Å^3 vs 219.4 Å^3), $TlFeO_3$ and $DyFeO_3$ (225.7 Å^3 vs 226.3 Å^3), and $TlNiO_3$ and $DyNiO_3$ (213.3 Å^3 vs 213.4 Å^3),[27,29] suggesting a revision[29] of the Shannon ionic radius of Tl^{3+}, which is currently close to that of Lu^{3+}.[31] Note that the deviation for $ScMnO_3$ and $(In_{0.889}Mn_{0.111})MnO_3$ likely results from their departure from trivalent character; $BiMnO_3$ follows the linear dependence of unit cell volume on *A*-site ionic size observed in the rest of the $RMnO_3$ family.

Next we compare the orbital ordering and resulting magnetic interactions. In all cases because of the d^4 orbital occupancy on the Mn^{3+} ions, each Mn^{3+} ion has four FM interactions and two AFM interactions. In $LaMnO_3$, the La^{3+} *A*-site ion is chemically inert, and the orbital ordering pattern (Figure 1) is determined by minimization of internal strains. The result is that all interactions are FM in the *ac* plane with FM (010) layers that are coupled antiferromagnetically along the *b* direction in an A-type AFM spin structure.[1] This symmetry permits weak ferromagnetism, which has been reported in $RMnO_3$ (*R* = La−Sm).[55] In $RMnO_3$ (*R* = Ho−Lu), the increased tilting of MnO_6 octahedra changes the relative orientations of the FM and AFM interactions resulting in the E-type AFM structure. This symmetry does not permit weak ferromagnetism, so $RMnO_3$ (*R* = Ho−Lu) are collinear antiferromagnets;[15] however, it breaks the inversion symmetry and results in electrical polarization.[15] In $BiMnO_3$, the stereochemically active

dx.doi.org/10.1021/ic501380m | Inorg. Chem. 2014, 53, 9800−9808

lone pair on the Bi^{3+} ion leads to a frustrated orbital ordering in which FM interactions dominate over the competing AFM ones[58] producing an overall FM spin structure with magnetic moments oriented along the monoclinic *b* direction.[59,60] At first glance, the orbital ordering pattern in $TlMnO_3$ looks similar to that of $BiMnO_3$, but closer examination shows that one AFM-FM pair is exchanged removing the frustration and allowing ferromagnetic arrangement of the magnetic moments along the [010] and [101] directions, with the antiferromagnetic ordering along the [−101] direction. There is no weak ferromagnetism as the symmetry does not allow canting. Regarding the ordering temperatures, the T_N of $TlMnO_3$ lies within the range of the lighter rare earth perovskite manganites, being closest to that of $PrMnO_3$. This is in contrast to other thallium compounds, for example, the T_N values of $TlFeO_3$ (T_N = 560 K) and $TlNiO_3$ (T_N = 105 K) are significantly smaller than even those of the heaviest rare earth compounds $LuFeO_3$ (T_N = 625 K) and $LuNiO_3$ (T_N = 130 K), respectively.[28,29]

Triclinic symmetry ($NaCuF_3$ structural type) is not common in perovskites, but is also observed in $BiNiO_3$ (at RT)[61] and $ScVO_3$ (below 90 K)[62] which have the same $a^+b^-c^-$ tilt patterns. However, the origin of the triclinic distortion in $BiNiO_3$ is the charge disproportionation on the Bi ions, to yield $Bi_{0.5}^{3+}Bi_{0.5}^{5+}Ni^{2+}O_3$.[61,63] In fact, above about 4 GPa at RT, the charge distribution in $BiNiO_3$ becomes the trivalent $Bi^{3+}Ni^{3+}O_3$, and the structure recovers the *Pnma* space group.[63] $Sc^{3+}V^{3+}O_3$ has space group *Pnma* down to 90 K;[62] the triclinic distortion below 90 K is believed to result from the very small size of the Sc^{3+} ions and independent tilts of the VO_6 octahedra. In comparison with the trivalent rare earth ions, Tl^{3+} ions prefer a highly asymmetric coordination with four very short Tl−O bonds. In spite of this preference, $TlCrO_3$, $TlFeO_3$, and $TlNiO_3$ adopt similar $GdFeO_3$-type structures to the corresponding $RCrO_3$, $RFeO_3$, and $RNiO_3$ families (there is a very weak monoclinic distortion in $TlNiO_3$ and $RNiO_3$ originating from charge disproportionation of Ni^{3+} ions).[27−30] We conclude, therefore, that the combination of the Jahn−Teller Mn^{3+} ions and covalency of the Tl−O bonds cooperate to produce the very strong structural distortion in $TlMnO_3$ that is stable in a wide temperature range from 2 to 820 K.

CONCLUSION

In conclusion, we prepared a new member of the $AMnO_3$ perovskite manganite family, $TlMnO_3$, using the high-pressure high-temperature technique and showed that its crystal structure (space group), magnetic structure, and orbital ordering are different from those of the previously known trivalent perovskite manganites. Using first-principles calculations with the HSE06 hybrid functional, we showed that the origin of these differences is covalent bonding between Tl 6s and Tl 6p and O 2p orbitals, which stabilizes a different orbital and magnetic ordering from the other members of the series. $TlMnO_3$ expands the $AMnO_3$ family from one hand. From another hand, it stands apart from other members of the family similar to $BiMnO_3$. Therefore, $TlMnO_3$ has potential to become a new playground in the manganite family.

ASSOCIATED CONTENT

Supporting Information

Structure parameters of $TlMnO_3$ obtained from synchrotron XRPD data, synchrotron XRPD patterns, DSC data and XRPD patterns after DSC, some additional results of the first-principle calculations, cif file (PDF). This material is available free of charge via the Internet at http://pubs.acs.org.

AUTHOR INFORMATION

Corresponding Author

*E-mail: Alexei.Belik@nims.go.jp.

Notes

The authors declare no competing financial interest.

ACKNOWLEDGMENTS

This work was supported by World Premier International Research Center Initiative (WPI Initiative, MEXT, Japan), the Japan Society for the Promotion of Science (JSPS) through its "Funding Program for World-Leading Innovative R&D on Science and Technology (FIRST Program)," the Grants-in-Aid for Scientific Research (22246083) from JSPS, Japan, the JSPS Postdoctoral Fellowships for Research Abroad, and the ETH Zürich. The synchrotron radiation experiments were performed at the SPring-8 with the approval of the Japan Synchrotron Radiation Research Institute (Proposal Nos. 2011B4512, 2012A4507, and 2011B4514).

REFERENCES

(1) Coey, J. M. D.; Viret, M.; von Molnar, S. *Adv. Phys.* **2009**, *58*, 571−697.
(2) Salamon, M. B.; Jaime, M. *Rev. Mod. Phys.* **2001**, *73*, 583−628.
(3) Rao, C. N. R.; Cheetham, A. K.; Mahesh, R. *Chem. Mater.* **1996**, *8*, 2421−2432.
(4) Rao, C. N. R.; Arulraj, A.; Cheetham, A. K.; Raveau, B. *J. Phys.: Condens. Matter* **2000**, *12*, R83−106.
(5) Edwards, D. M. *Adv. Phys.* **2002**, *51*, 1259−1318.
(6) Ramirez, A. P. *J. Phys.: Condens. Matter* **1997**, *9*, 8171−8199.
(7) Topfer, J.; Goodenough, J. B. *J. Solid State Chem.* **1997**, *130*, 117−128.
(8) Maurin, I.; Barboux, P.; Lassailly, Y.; Boilot, J. P.; Villain, F.; Dordor, P. *J. Solid State Chem.* **2001**, *160*, 123−133.
(9) Huang, Q.; Santoro, A.; Lynn, J. W.; Erwin, R. W.; Borchers, J. A.; Peng, J. L.; Greene, R. L. *Phys. Rev. B* **1997**, *55*, 14987−14999.
(10) Kimura, T.; Goto, T.; Shintani, H.; Ishizaka, K.; Arima, T.; Tokura, Y. *Nature (London)* **2003**, *426*, 55−58.
(11) Fiebig, M.; Lottermoser, T.; Frohlich, D.; Goltsev, A. V.; Pisarev, R. V. *Nature (London)* **2002**, *419*, 818−820.
(12) Lee, S.; Pirogov, A.; Kang, M. S.; Jang, K. H.; Yonemura, M.; Kamiyama, T.; Cheong, S. W.; Gozzo, F.; Shin, N.; Kimura, H.; Noda, Y.; Park, J. G. *Nature (London)* **2008**, *451*, 805−809.
(13) Kumagai, Y.; Belik, A. A.; Lilienblum, M.; Leo, N.; Fiebig, M.; Spaldin, N. A. *Phys. Rev. B* **2012**, *85*, 174422.
(14) Tachibana, M.; Shimoyama, T.; Kawaji, H.; Atake, T.; Takayama-Muromachi, E. *Phys. Rev. B* **2007**, *75*, 144425.
(15) Pomjakushin, V. Yu.; Kenzelmann, M.; Doenni, A.; Harris, A. B.; Nakajima, T.; Mitsuda, S.; Tachibana, M.; Keller, L.; Mesot, J.; Kitazawa, H.; Takayama-Muromachi, E. *New J. Phys.* **2009**, *11*, 043019.
(16) Glazer, A. M. *Acta Crystallogr., Sect. B* **1972**, *28*, 3384−3392.
(17) Howard, C. J.; Stokes, H. T. *Acta Crystallogr. Sect., B* **1998**, *54*, 782−789.
(18) Belik, A. A.; Iikubo, S.; Yokosawa, T.; Kodama, K.; Igawa, N.; Shamoto, S.; Azuma, M.; Takano, M.; Kimoto, K.; Matsui, Y.; Takayama-Muromachi, E. *J. Am. Chem. Soc.* **2007**, *129*, 971−977.
(19) Belik, A. A. *J. Solid State Chem.* **2012**, *195*, 32−40.
(20) Baettig, P.; Seshadri, R.; Spaldin, N. A. *J. Am. Chem. Soc.* **2007**, *129*, 9854−9855.
(21) Belik, A. A.; Matsushita, Y.; Tanaka, M.; Takayama-Muromachi, E. *Angew. Chem., Int. Ed.* **2010**, *49*, 7723−7727.
(22) Chen, H. Y.; Yu, T.; Gao, P.; Bai, J. M.; Tao, J.; Tyson, T. A.; Wang, L.; Lalancette, R. *Inorg. Chem.* **2013**, *52*, 9692−9697.

(23) Ovsyannikov, S. V.; Abakumov, A. M.; Tsirlin, A. A.; Schnelle, W.; Egoavil, R.; Verbeeck, J.; Van Tendeloo, G.; Glazyrin, K. V.; Hanfland, M.; Dubrovinsky, L. *Angew. Chem., Int. Ed.* **2013**, *52*, 1494−1498.
(24) Belik, A. A.; Yi, W. *J. Phys.: Condens. Matter* **2014**, *26*, 163201.
(25) Uusi-Esko, K.; Malm, J.; Imamura, N.; Yamauchi, H.; Karppinen, M. *Mater. Chem. Phys.* **2008**, *112*, 1029−1034.
(26) Yu, T.; Gao, P.; Wu, T.; Tyson, T. A.; Lalancette, R. *Appl. Phys. Lett.* **2013**, *102*, 172901.
(27) Shannon, R. D. *Inorg. Chem.* **1967**, *6*, 1474−1478.
(28) (a) Kim, S. J.; Demazeau, G.; Presniakov, I.; Choy, J. H. *J. Solid State Chem.* **2001**, *161*, 197−204. (b) Presniakov, I. A.; Sobolev, A. V.; Baranov, A. V.; Demazeau, G.; Rusakov, V. S. *J. Phys.: Condens. Matter* **2006**, *18*, 8943−8959.
(29) Kim, S. J.; Demazeau, G.; Alonso, J. A.; Choy, J. H. *J. Mater. Chem.* **2001**, *11*, 487−492.
(30) Kim, S. J.; Martinez-Lope, M. J.; Fernandez-Diaz, M. T.; Alonso, J. A.; Presniakov, I.; Demazeau, G. *Chem. Mater.* **2002**, *14*, 4926−4932.
(31) Shannon, R. D. *Acta Crystallogr., Sect. A* **1976**, *32*, 751−767.
(32) Viskov, A. S.; Zubova, E. V.; Burdina, K. P.; Venevtsev, Yu. N. *Sov. Phys. Crystallogr.* **1971**, *15*, 932−934 (*Kristallografiya* **1970**, *15*, 1071−1073 (in Russian)).
(33) Tanaka, M.; Katsuya, Y.; Yamamoto, A. *Rev. Sci. Instrum.* **2008**, *79*, 075106.
(34) Izumi, F.; Ikeda, T. *Mater. Sci. Forum* **2000**, *321−324*, 198−203.
(35) SMART, Molecular analysis research tool; Bruker AXS Inc., Madison, WI, 2001.
(36) SAINT, Data reduction and correction program; Bruker AXS Inc., Madison, WI, 2001.
(37) SADABS, An empirical absorption correction program; Bruker AXS Inc.: Madison, WI, 2001.
(38) Sheldrick, G. M. *Acta Crystallogr., Sect. A* **2008**, *64*, 112−122.
(39) Farrugia, L. J. *J. Appl. Crystallogr.* **1999**, *32*, 837−838.
(40) Matsnev, M. E.; Rusakov, V. S. *AIP Conf. Proc.* **2012**, *1489*, 178−185.
(41) (a) Blöchl, P. E. *Phys. Rev. B* **1994**, *50*, 17953−17979. (b) Kresse, G.; Joubert, J. *Phys. Rev. B* **1999**, *59*, 1758−1775.
(42) (a) Kresse, G.; Hafner, J. *Phys. Rev. B* **1993**, *47*, 558−561. (b) Kresse, G.; Furthmüller, J. *Comput. Mater. Sci.* **1996**, *6*, 15−50.
(43) (a) Heyd, J.; Scuseria, G.; Ernzerhof, M. *J. Chem. Phys.* **2003**, *118*, 8207−8215. (b) Krukau, V.; Vydrov, O. A.; Izmaylov, A. F.; Scuseria, G. E. *J. Chem. Phys.* **2006**, *125*, 224106.
(44) Stroppa, A.; Marsman, M.; Kresse, G.; Picozzi, S. *New J. Phys.* **2010**, *12*, 093026.
(45) Hong, J.; Stroppa, A.; Iniguez, J.; Picozzi, S.; Vanderbilt, D. *Phys. Rev. B* **2012**, *85*, 054417.
(46) Akamatsu, H.; Kumagai, Y.; Oba, F.; Fujita, K.; Murakami, H.; Tanaka, K.; Tanaka, I. *Phys. Rev. B* **2011**, *83*, 214421.
(47) Akamatsu, H.; Kumagai, Y.; Oba, F.; Fujita, K.; Tanaka, K.; Tanaka, I. *Adv. Funct. Mater.* **2013**, *23*, 1864−1872.
(48) Kumagai, Y.; Soda, Y.; Oba, F.; Seko, A.; Tanaka, I. *Phys. Rev. B* **2012**, *85*, 033203.
(49) Brese, R. E.; O'Keeffe, M. *Acta Crystallogr., Sect. B* **1991**, *47*, 192−197.
(50) Rodríguez-Carvajal, J.; Hennion, M.; Moussa, F.; Moudden, A. H.; Pinsard, L.; Revcolevschi, A. *Phys. Rev. B* **1998**, *57*, 3189−3192(R).
(51) Zhou, J. S.; Goodenough, J. B. *Phys. Rev. B* **1999**, *60*, 15002−15004(R).
(52) Zhou, J. S.; Goodenough, J. B. *Phys. Rev. Lett.* **2006**, *96*, 247202.
(53) Ramirez, A. P.; Subramanian, M. A. *Science* **1997**, *277*, 546−549.
(54) Raju, N. P.; Greedan, J. E.; Subramanian, M. A. *Phys. Rev. B* **1994**, *49*, 1086−1091.
(55) Ritter, C.; Ibarra, M. R.; De Teresa, J. M.; Algarabel, P. A.; Marguina, C.; Blasco, J.; Garcia, J.; Oseroff, S.; Cheong, S. W. *Phys. Rev. B* **1997**, *56*, 8902−8911.
(56) Belik, A. A.; Takayama-Muromachi, E. *Inorg. Chem.* **2007**, *46*, 5585−5590.
(57) Fennie, C. J.; Ederer, C. *J. Phys.: Condens. Matter* **2008**, *20*, 434219.
(58) Yang, C. H.; Koo, T. Y.; Lee, S. H.; Song, C.; Lee, K. B.; Jeong, Y. H. *Europhys. Lett.* **2006**, *74*, 348−354.
(59) Moreira dos Santos, A.; Cheetham, A. K.; Atou, T.; Syono, Y.; Yamaguchi, Y.; Ohoyama, K.; Chiba, H.; Rao, C. N. R. *Phys. Rev. B* **2002**, *66*, 064425.
(60) Montanari, E.; Calestani, G.; Righi, L.; Gilioli, E.; Bolzoni, F.; Knight, K. S.; Radaelli, P. G. *Phys. Rev. B* **2007**, *75*, 220101(R).
(61) Ishiwata, S.; Azuma, M.; Takano, M.; Nishibori, E.; Takata, M.; Sakata, M.; Kato, K. *J. Mater. Chem.* **2002**, *12*, 3733−3373.
(62) Castillo-Martinez, E.; Bieringer, M.; Shafi, S. P.; Cranswick, L. M. D.; Alario-Franco, M. A. *J. Am. Chem. Soc.* **2011**, *133*, 8552−8563.
(63) Azuma, M.; Carlsson, S.; Rodgers, J.; Tucker, M. G.; Tsujimoto, M.; Ishiwata, S.; Isoda, S.; Shimakawa, Y.; Takano, M.; Attfield, J. P. *J. Am. Chem. Soc.* **2007**, *129*, 14433−14436.